JOINT INSTITUTE FOR NUCLEAR RESEARCH
Laboratory of Radiation Biology

FINAL REPORT ON THE INTEREST PROGRAMME

Calculation of radiation dose and radiolytic species distributions within Bragg peak region of therapeutic proton beams

Supervisor:
Dr Batmunkh Munkhbaatar

Student:
Marry Thekhwe
South Africa
University of Cape Town

Participation period:
March 05 - April 20, 2026 (Wave 14)

Abstract

This project investigated proton interactions in water using Geant4 simulations. Depth-dose profiles were generated for 70 MeV and 227 MeV proton beam energies to examine Bragg peak formation and range differences in water. Then track structure was visualised to understand how energy is deposited in proton beams, and the radial dose distribution for a 1 MeV proton was calculated and compared with experimental data. In addition, the time evolution of selected radiolytic species, namely e_{aq}^-, $^\bullet OH$, H_2O_2, $HO_2^\bullet$, O_2^-, and $^\bullet H$, was analysed through G-values as a function of time. The results reproduced the expected Bragg peak behaviour, showed clustered ionisation patterns along the proton track, and demonstrated a decreasing radial dose trend with increasing distance from the track core. The project provided a review of proton energy deposition and early radiolytic processes in water.

1 Introduction

Ionising radiation deposits energy in matter through a sequence of events that begins at extremely short timescales and extends into later chemical evolution. In biological media, where water is the dominant component, the earliest interactions are governed primarily by excitation, ionisation, and the production of secondary electrons. These initial events form the basis of water radiolysis. Short-lived reactive species such as hydroxyl radicals ($^{\bullet}OH$), hydrated electrons (e^{-}_{aq}), hydrogen atoms ($^{\bullet}H$), and, in oxygen-containing systems, oxygen-derived radicals such as $HO_2^{\bullet}$ and O_2^{-} are produced. More stable molecular products such as H_2O_2 can then emerge through subsequent diffusion-controlled reactions [1, 2].

For charged particles such as protons, the spatial pattern of energy deposition is highly non-uniform. At the macroscopic scale, protons exhibit the well-known Bragg peak, where the dose increases toward the end of the particle range. At the microscopic scale, the same transport process gives rise to clustered ionisation events along and around the particle track. These microscopic patterns are important because they influence the local physicochemical environment in which radiolytic species are formed and evolve. A full interpretation of proton interactions therefore benefits from a multi-scale approach that links depth-dose behaviour, track structure, radial energy deposition, and radiolytic yields.

Monte Carlo track-structure simulation provides a suitable framework for this purpose. Geant4 and its Geant4-DNA extension allow particle interactions in liquid water to be simulated down to very low energies, while also enabling the modelling of early radiation chemistry through reaction networks based on experimentally established diffusion coefficients and rate constants [3, 4, 5, 6]. In this project, these capabilities were used to investigate proton energy deposition in water at both macroscopic and microscopic scales, and to analyse the time evolution of selected radiolytic species produced after irradiation.

2 Project Goals

The main goal of this project was to investigate proton interactions in water using Monte Carlo simulation.

The specific objectives were:

- to simulate proton depth-dose distributions and reproduce Bragg peak behaviour at clinically relevant energies,
- to visualise proton track structure in liquid water at micrometric and nanometric scales,
- to calculate the radial dose distribution around a proton track and compare the simulated trend with experimental data,
- to evaluate the time-dependent G-values of selected radiolytic species generated in water following proton irradiation.

Taken together, these objectives were intended to provide a coherent picture of how proton energy deposition in water can be interpreted from the physical stage through to the chemical stage.

3 Scope of the Project

The scope of this project included the setup, execution, and analysis of proton transport and radiolysis simulations in Geant4. The work covered both macroscopic and microscopic aspects of radiation interaction in water. At the macroscopic level, simulations were performed to generate depth-dose curves for proton beams at 70 MeV and 227 MeV in order to study Bragg peak formation and range differences. At the microscopic level, track-structure simulations were carried out in liquid water to examine localised interaction patterns along the proton path. These simulations were further used to calculate the radial dose distribution for a 1 MeV proton and to compare the resulting trend with experimental data.

The chemical stage of water radiolysis was investigated through the time evolution of six selected species: e_{aq}^-, $^\bullet OH$, H_2O_2, $HO_2^\bullet$, O_2^-, and $^\bullet H$. The project therefore focused on linking proton transport, microscopic energy deposition, and early radiolytic chemistry within a single simulation-based study.

4 Method and Simulation Setup

4.1 Method

When ionising radiation passes through water, it deposits energy through discrete interactions with water molecules. These interactions can be described in terms of three connected stages: the physical stage, the physico-chemical stage, and the chemical stage [1, 2].

1. **Physical stage:** During the earliest stage, the incident proton and the secondary electrons it produces lose energy through excitation and ionisation of water molecules. This occurs on femtosecond timescales. Typical processes include

$$H_2O \longrightarrow H_2O^+ + e^- \tag{1}$$

and

$$H_2O \longrightarrow H_2O^*. \tag{2}$$

2. **Physico-chemical stage:** The ionised and excited water molecules are unstable and rapidly transform into reactive intermediates. For example,

$$H_2O^+ + H_2O \longrightarrow H_3O^+ + {}^\bullet OH \tag{3}$$
$$H_2O^* \longrightarrow {}^\bullet H + {}^\bullet OH \tag{4}$$

while low-energy electrons thermalise and become solvated:

$$e^- \longrightarrow e_{aq}^-. \tag{5}$$

3. **Chemical stage:** After thermalisation and solvation, the radiolytic species diffuse and react with one another. These reactions can lead to the formation of both radical and molecular products. Representative reactions include

$$^\bullet OH + {}^\bullet OH \longrightarrow H_2O_2 \tag{6}$$
$$^\bullet H + O_2 \longrightarrow HO_2^\bullet \tag{7}$$
$$e_{aq}^- + O_2 \longrightarrow O_2^-. \tag{8}$$

In this project, the physical stage was used to study proton transport, depth-dose deposition, and track structure, while the chemical stage was used to analyse the temporal evolution of selected radiolytic species. The overall methodology therefore linked large-scale proton dose deposition with the local structure of energy release and its chemical consequences in water.

Table 1 lists the principal species considered in the chemistry analysis.

Species formula	**Name**
$^{\bullet}OH$	Hydroxyl radical
e^{-}_{aq}	Hydrated electron
$^{\bullet}H$	Hydrogen atom
$HO_2^{\bullet}$	Hydroperoxyl radical
O_2^{-}	Superoxide radical anion
H_2O_2	Hydrogen peroxide

Table 1: Radiolytic species analysed in this project.

4.2 Simulation Geometry

Two simulations were considered for this project. For the track-structure and radiolysis calculations, the geometry consisted of a homogeneous liquid-water volume defined using the Geant4-DNA water material. A micrometric water box was used so that the proton track, local energy deposition events, and the subsequent formation of radiolytic species could be followed within a controlled volume.

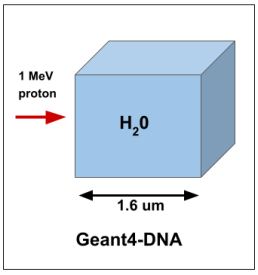

Figure 1: 1.6 µm liquid water box irradiated by 1 MeV protons which was used for the track structures simulations.

For the depth-dose calculations, a larger water phantom was used to allow full proton transport and the development of the Bragg peak over clinically relevant penetration depths. This larger-scale geometry was necessary because the 70 MeV and 227 MeV proton beams have markedly different ranges in water as to where they and stop and deposit most of their energies resulting in Bragg peak formation. Thus, while the material composition remained water throughout the study, the geometric scale was adapted to the quantity of interest, a small geometry as seen in figure 1 for track-structure and chemistry simulations, and a much larger phantom for Bragg peak simulations.

4.3 Software and Physics-Chemistry Configuration

All simulations were carried out using the Geant4 Monte Carlo toolkit together with the Geant4-DNA extension for track-structure and chemistry modelling [3, 4]. Geant4 provided the transport, geometry, and scoring framework, while Geant4-DNA enabled detailed modelling of low-energy interactions in liquid water and the subsequent radiolysis chemistry.

The simulation workflow included:

- proton transport in water for depth-dose and track-structure calculations,
- event-by-event scoring of microscopic energy deposition,
- post-processing of the deposited energy to obtain radial dose distributions,
- time-dependent chemistry calculations for selected radiolytic species.

For the chemistry stage, the Geant4-DNA radiolysis reaction network was used. This framework models the diffusion and reactions of water radiolysis products using reaction schemes and kinetic data based on established radiation-chemistry literature [2, 5, 6].

4.4 Particle Source

Protons were used as the primary particles throughout the project. Three proton energies were selected depending on the quantity being studied. For the macroscopic depth-dose calculations, proton beams of 70 MeV and 227 MeV were simulated in order to examine Bragg peak formation at different penetration ranges. For the microscopic radial dose and chemistry calculations, a 1 MeV proton was used. This lower energy is relevant for studying dense local energy deposition and short-range track-structure behaviour, and it is useful for probing conditions associated with the slowing-down part of the proton track.

4.5 Depth-Dose and Bragg Peak Analysis

The absorbed dose was obtained from the energy deposited in scoring regions of known mass:

$$D = \frac{\Delta E}{\Delta m}. \tag{9}$$

Depth-dose curves were then constructed by scoring the deposited energy as a function of depth in water and normalising the values to percentage depth dose. This allowed the position and qualitative shape of the Bragg peak to be compared for the two proton energies.

4.6 Radial Dose Distribution

The radial dose distribution was calculated from microscopic energy-deposition data scored around the proton track. The perpendicular distance from the beam axis was first determined as

$$r = \sqrt{x^2 + y^2}, \tag{10}$$

where x and y are the transverse coordinates relative to the proton beam axis.

The deposited energy was then accumulated in concentric cylindrical shells around the track. For each shell, the dose was calculated by dividing the deposited energy by the mass of that shell:

$$D(r) = \frac{E_{\text{dep}}(r)}{m(r)}. \tag{11}$$

This approach yields the radial variation of deposited dose away from the proton track core and provides a direct way to compare simulation results with experimentally derived radial-dose trends.

4.7 Track Structure Visualisation

To visualise the microscopic structure of proton interactions, the coordinates of individual energy-deposition events were recorded and plotted in three dimensions. These plots provide a qualitative representation of the proton track and reveal how interactions cluster spatially along the particle path.

4.8 G-values and Chemical Analysis

The radiation chemical yield, or G-value, expresses the number of molecules of a given species produced or lost per 100 eV of absorbed energy. It was calculated as

$$G_i(t) = \frac{N_i(t)}{E_{\text{abs}}} \times 100 \text{ eV}, \tag{12}$$

where $N_i(t)$ is the number of molecules of species i at time t, and E_{abs} is the total absorbed energy.

In this project, time-dependent G-values were analysed for the species e_{aq}^-, $^\bullet OH$, H_2O_2, $HO_2^\bullet$, O_2^-, and $^\bullet H$. These species were selected because they represent both short-lived reactive intermediates and longer-lived chemical products relevant to water radiolysis.

4.9 Data Collection and Analysis

Simulation outputs were processed to obtain:

- depth-dose curves for the 70 MeV and 227 MeV proton beams,
- three-dimensional proton track visualisations,
- radial dose distributions for a 1 MeV proton,
- G-value curves as a function of time for the selected radiolytic species.

Post-processing and plotting were performed using ROOT and Python. These tools were used to organise the scored data, calculate derived quantities such as radial dose, and generate the final plots presented in the report.

5 Results

5.1 Macroscopic Dose Deposition: Bragg Peak Profiles

The depth-dose distributions for proton beams at energies of 70 MeV and 227 MeV were simulated using Geant4. The results are shown in Figures 2 and 3.

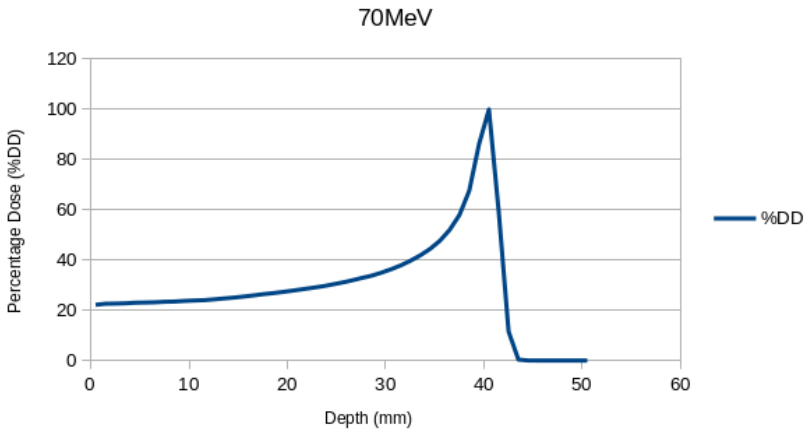

Figure 2: Depth-dose profile for a 70 MeV proton beam showing a pronounced Bragg peak near the end of range.

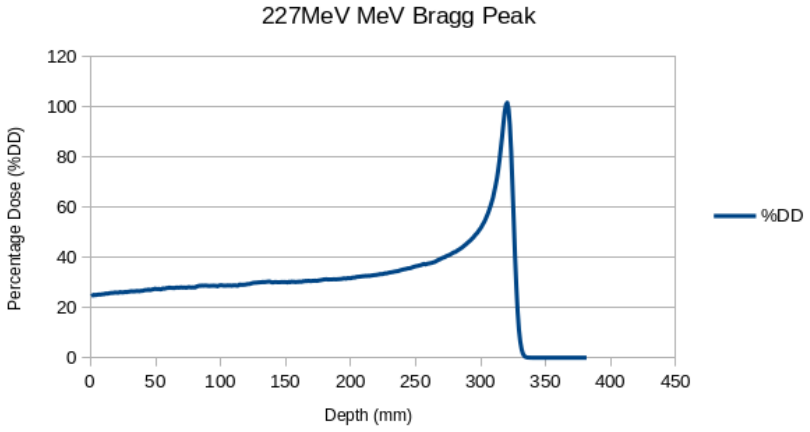

Figure 3: Depth-dose profile for a 227 MeV proton beam illustrating increased penetration depth and distal fall-off.

The simulated depth-dose curves exhibit the characteristic Bragg peak behaviour of charged particles, where energy deposition increases with depth and reaches a maximum near the end of the particle range [7]. The 227 MeV beam penetrates significantly deeper than the 70 MeV beam, consistent with theoretical expectations based on stopping power.

5.2 Microscopic Track Structure

The three-dimensional track structure of a proton simulated with Geant4-DNA is shown in Figure 4.

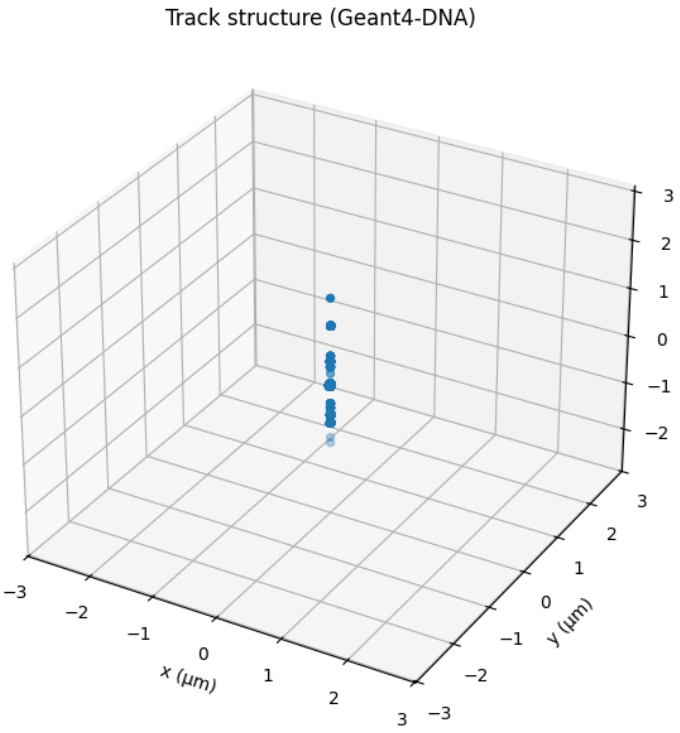

Figure 4: Three-dimensional proton track showing clustered ionisation events.

The spatial distribution of interaction points demonstrates the stochastic nature of radiation interactions at the nanometric scale. Ionisation events are concentrated along the particle trajectory, forming clusters that are relevant for biological damage mechanisms [8].

5.3 Radial Dose Distribution

The radial dose distribution for a 1 MeV proton was calculated and compared with experimental data, as shown in Figure 5.

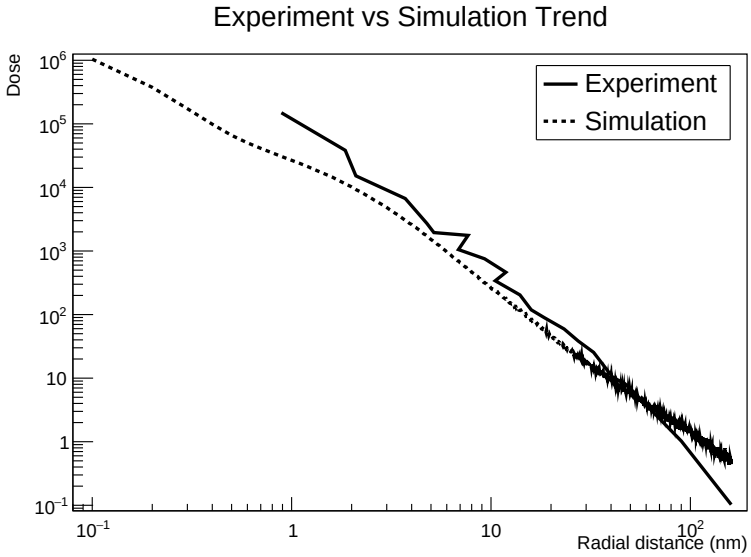

Figure 5: Comparison between simulated and experimental radial dose distributions, experimental data from Dr Batmunkh(private communication).

The results show a rapid decrease in dose with increasing radial distance from the track core. This behaviour is consistent with the physics of secondary electron transport, where low-energy electrons deposit energy close to the primary track [9]. The simulation reproduces the general trend observed experimentally, although differences in magnitude and range are observed.

5.4 Radiochemical Evolution: G-values

The time evolution of radiolytic species is shown in Figure 6.

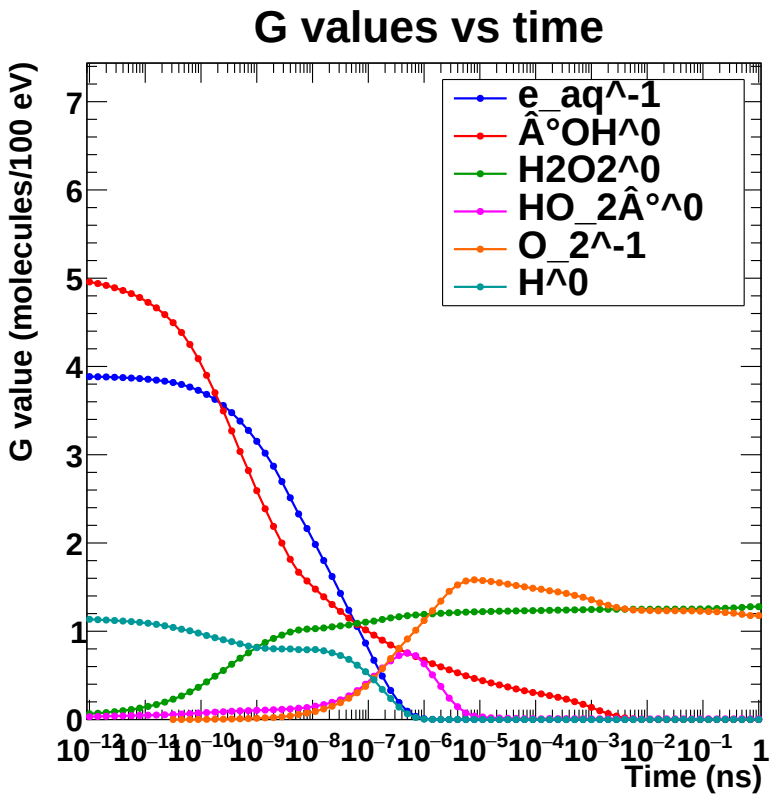

Figure 6: G-values of selected radiolytic species as a function of time.

At early times, reactive species such as solvated electrons (e^-_{aq}) and hydroxyl radicals ($\cdot OH$) dominate due to primary ionisation processes. Over time, recombination reactions lead to the formation of more stable species such as hydrogen peroxide (H_2O_2) [10]. These results demonstrate the coupling between physical and chemical stages of radiation interaction.

6 Discussion

The results obtained in this study demonstrate that Geant4 and Geant4-DNA are capable of modelling radiation interactions across multiple spatial and temporal scales, from macroscopic dose deposition to microscopic track structure and chemical evolution. The Bragg peak results for 70 MeV and 227 MeV protons are consistent with theoretical expectations and previously reported simulations [7]. The increase in penetration depth with energy and the sharp distal fall-off confirm that the simulation correctly models proton stopping power and energy loss processes.

At the microscopic level, the track structure simulations reveal clustered ionisation events along the particle trajectory. This clustering is a key feature of high-LET radiation and plays an important role in determining biological effectiveness [11]. The observed spatial distribution is therefore physically meaningful and supports the validity of the Geant4-DNA physics models.

The radial dose distribution shows good qualitative agreement with experimental data, particularly in the rapid decrease of dose with radial distance. However, discrepancies

between simulation and experiment are evident. One major limitation is the limited radial extent of the simulation data compared to the experimental measurements. This is likely due to insufficient statistics and the limited number of simulated primary particles. Increasing the number of simulated events would improve the smoothness and range of the distribution.

Additional sources of discrepancy may include:

- Simplifications in the geometry and material composition
- Limitations in the Geant4-DNA cross-section models
- Differences in experimental conditions not reproduced in the simulation

The G-value results provide insight into the chemical stage of radiation interaction. The temporal evolution of species such as e^-_{aq} and $\cdot OH$ follows expected trends, with early-time dominance of reactive species followed by recombination into more stable molecules such as H_2O_2 [10]. This confirms that the chemical stage is being modelled consistently.

One limitation of the current study is that only a single proton energy (1 MeV) was used for microscopic and chemical analysis. In reality, proton energy varies along the track, particularly near the Bragg peak, where LET is significantly higher. Future work should include simulations at multiple energies corresponding to different depths in the Bragg curve. The results demonstrate a consistent and physically meaningful link between macroscopic dose deposition, microscopic track structure, and radiochemical processes. This multi-scale modelling approach is essential for understanding radiation effects in biological systems.

7 Conclusion

In this study, Monte Carlo simulations using Geant4 and Geant4-DNA were employed to investigate radiation interactions, for Geant4 simulations we successfully reproduced the characteristic Bragg peak behaviour for proton beams at different energies, confirming accurate modelling of energy deposition in matter. For Geant4-DNA track structure simulations revealed clustered ionisation events consistent with the stochastic nature of radiation interactions.

The radial dose distribution demonstrated qualitative agreement with experimental data, highlighting the capability of the simulation to model energy deposition around particle tracks. The analysis of G-values further showed the time-dependent evolution of radiolytic species, linking physical interactions to chemical processes. Despite some discrepancies between simulation and experiment, primarily due to statistical limitations and modelling assumptions, the overall agreement supports the validity of the simulation framework. This work demonstrates the potential of Geant4-DNA for radiation modelling and provides a foundation for future studies investigating biological effects and applications such as proton therapy and FLASH radiotherapy.

Acknowledgments

I would like to sincerely thank my project supervisor for always being available when I needed guidance, for explaining complex concepts in a way I could understand, and for

supporting me throughout this learning journey. I would also like to thank my supervisors from my home university for their encouragement and continued support. Finally, I am grateful to the INTEREST programme organisers for this wonderful initiative, which fosters growth, development, and collaboration.

References

[1] Ans Baeyens, Ana Margarida Abrantes, Vidhula Ahire, et al. Basic concepts of radiation biology. In Sarah Baatout, editor, *Radiobiology Textbook*, pages 25–81. Springer, Cham, 2023.

[2] George V. Buxton, Clive L. Greenstock, William P. Helman, and Alberta B. Ross. Critical review of rate constants for reactions of hydrated electrons, hydrogen atoms and hydroxyl radicals ($^{\bullet}OH/O^{-}$) in aqueous solution. *Journal of Physical and Chemical Reference Data*, 17(2):513–886, 1988.

[3] S. Agostinelli et al. Geant4—a simulation toolkit. *Nuclear Instruments and Methods in Physics Research Section A*, 506(3):250–303, 2003.

[4] S. Incerti et al. The geant4-dna project. *International Journal of Modeling, Simulation, and Scientific Computing*, 1(2):157–178, 2010.

[5] S. Incerti, I. Kyriakou, M. A. Bernal, et al. Geant4-dna example applications for track structure simulations in liquid water: A report from the geant4-dna project. *Medical Physics*, 45(8):e722–e739, 2018.

[6] Woo Gyu Shin, José Ramos-Méndez, Ioanna Kyriakou, et al. Review of chemical models and applications in geant4-dna at the dawn of the exascale era. *Medical Physics*, 2024.

[7] Harald Paganetti. *Proton Therapy Physics*. CRC Press, 2012.

[8] S. et al. Incerti. The geant4-dna project. *International Journal of Modeling, Simulation, and Scientific Computing*, 1(2):157–178, 2010.

[9] W. et al. Friedland. Track structure simulations of ion interactions with biological targets. *Radiation and Environmental Biophysics*, 50:1–16, 2011.

[10] S. et al. Incerti. Simulation of radiation-induced chemical processes using geant4-dna. *Medical Physics*, 45(8):e722–e739, 2018.

[11] W. et al. Friedland. Dna damage induced by ionizing radiation. *Mutation Research*, 770:116–130, 2017.